On the Microstructure of a Freeze Lining of an Industrial Nonferrous Slag

MIEKE CAMPFORTS, KAREL VERSCHEURE, EDDY BOYDENS, TIM VAN ROMPAEY, BART BLANPAIN, and PATRICK WOLLANTS

Labscale freeze layers of an industrial nonferrous slag with Al_2O_3-CaO-FeO_x-MgO-SiO_2-ZnO as main components are studied to explore the microstructure and the composition of an industrial freeze lining. The freeze layers were formed by submerging a watercooled probe into a liquid slag bath. The influence of submergence time, of heat input from the furnace, and of the rotational speed of the crucible is studied. The microstructures of the freeze layers are examined using scanning electron microscopy (SEM), electron probe microanalysis (EPMA), and X-ray diffraction (XRD). Thermodynamic software is used to interpret the solidification microstructure. The results show that the freeze layer microstructure consists of different zones, depending on the local thermal history. These zones show different growth morphologies and different microstructure scales, from an amorphous matrix with small crystals to large columnar crystals. Furthermore, two microstructure types are observed, one with melilite columnar crystals and the other with olivine columnar crystals. These microstructure types appear for similar experimental conditions and are even observed within the same freeze layer. An increase in submergence time or in heat input from the slag bath does not seem to favor a particular microstructure type. A high rotational speed of the crucible resulting in a higher convection in the slag bath seems to favor the microstructure type with olivine columnar crystals.

I. INTRODUCTION

SEVERAL pyrometallurgical processes operate with high-intensity conditions, such as a high process temperature, a strong convection in the bath, and aggressive process materials. Examples are slag cleaning,[1,2] zinc fuming,[3,4] ilmenite smelting,[5–7] and the Hall–Héroult process.[8–11] These processes pose challenges related to reactor integrity and the life of the refractory reactor wall. To limit the corrosion of the refractory wall and extend its life, the wall is often cooled. As a result, a solid crust of process material, also referred to as a freeze lining, a freeze layer, or a side ledge, may form on the hot side of the refractory wall. In some processes, such as ilmenite smelting and the Hall–Héroult process, a freeze lining is even the best solution for reaching an acceptable campaign time.[6–9]

A freeze lining is the result of a thermal balance between the heat input from the liquid bath and the heat removal by the cooling medium, as is illustrated in Figure 1. In steady state, the heat input equals the heat removal and the freeze lining thickness remains constant. Any unbalance between the heat input and the heat removal results in the growth or melting of the freeze lining to re-establish steady state at another thickness. Furthermore, industrial process materials are often multicomponent systems. Therefore, the freeze lining composition may not equal the composition of the bath material. In this case, components have to be exchanged between the freeze lining and the bath, when the freeze lining grows or melts. Thus, the growth of the freeze lining can be a complex combination of mass transport and heat transport.

Because the process materials in the high-intensity processes are highly corrosive for the refractory wall, the formation of a freeze layer has to be guaranteed. The process material has to form a layer of solids on the reactor wall. Furthermore, this layer has to remain attached to the refractory wall and, ideally, does not spall. If the layer does spall, a new layer should form immediately. A better understanding of freeze lining behavior is thus necessary to establish the process conditions for an optimal protection of the refractory wall. The microstructure of the freeze layer contains information on the freeze layer formation and determines its physical, mechanical, and chemical properties, and therefore is very meaningful.

The microstructure of a freeze lining has been studied for cryolite salts of the Hall–Héroult process[8,9] and for some industrial nonferrous slags.[12] In the Hall–Héroult cell, the microstructure of the freeze lining is strongly dependent on the solidification rate.[8,9] At high solidification rates, an amorphous freeze layer forms with a composition close to the slag bath, while at intermediate

MIEKE CAMPFORTS, Research Assistant, and BART BLANPAIN and PATRICK WOLLANTS, Full Professors, are with the Centre for High Temperature Processes, Department of Metallurgy and Materials Engineering, Katholieke Universiteit Leuven, B-3001 Leuven, Belgium. Contact e-mail: Mieke.Campforts@mtm.kuleuven.be. KAREL VERSCHEURE and TIM VAN ROMPAEY, Project Leaders, and EDDY BOYDENS, Manager Analytical Laboratory, are with Umicore Research, B-2250 Olen, Belgium.
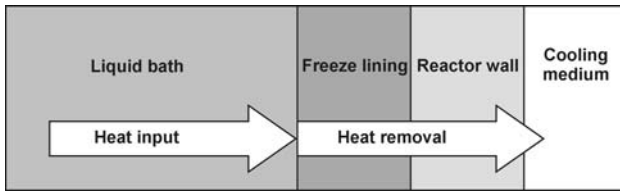
Fig. 1—Schematic representation of the heat transport in a freeze lining.

cooling rates, dendrites of primary phase form, entrapping bath material between the dendrites.[8,9] The composition of the freeze layer will vary from the primary phase, according to the phase diagram at low solidification rates to the bath composition at high rates. Clearly, the solidification rate influences the mass transport of components between the freeze layer and the bath. The freeze lining microstructure of the industrial nonferrous slags is also dependent on the solidification rate.[12] For high cooling rates, an amorphous phase forms; for intermediate cooling rates, columnar crystals form. Contrary to the cryolite salt freeze lining, the composition of the slag freeze lining is more or less constant for high to intermediate cooling rates, and equals the bath composition. The research on the microstructure of slag freeze lining is still explorative. Important issues include the freeze layer formation mechanisms and the influence of process conditions on the freeze layer formation.

The goal of this research is to study the microstructure and the composition of labscale freeze linings of an industrial nonferrous slag. The freeze layers are formed with a watercooled probe technique under different experimental conditions (varying submergence time, heat input, or rotational speed), to study the freeze lining formation, the influence of heat input from the slag bath, and the influence of convection in the slag bath.

II. EXPERIMENTAL

A. Watercooled Probe Technique

The experimental setup is shown in Figure 2. A 30-kW open induction furnace heats a SiC crucible containing a second crucible with the slag. Bath temperatures up to 1500 °C are achievable. The crucibles are placed on a rotational disk, with variable speed from 0 to 28.5 rpm. A watercooled probe is submerged into the molten slag, to form a freeze layer. The probe is made of stainless steel and its design is shown in Figure 3. The cooling water enters the probe through the inner tube (7.5 mm in diameter) and is evacuated through the outer tube (15 mm in diameter, 600 mm in length). Two thermocouples are attached, at 1 and 2 cm from the probe's surface (Figure 2, item 3). A removable thermocouple is used to measure the slag bath temperature before and after submerging the probe. This setup is similar to the one used in previous research.[12]

The experimental procedure is as follows: a SiC crucible containing an Al_2O_3 crucible with 3 kg of crushed slag (4 to 28 mm) is heated in the inductive
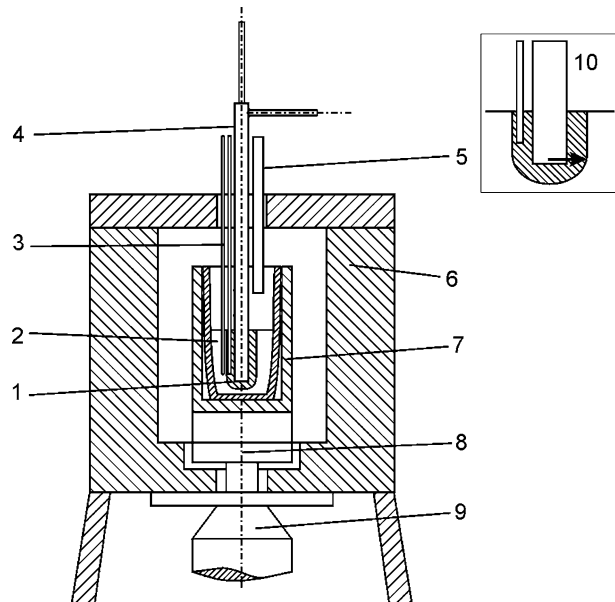

Fig. 2—Schematic drawing of the experimental setup: 1. freeze layer, 2. liquid slag bath, 3. thermocouples fixed to the probe at a constant distance from the probe's surface, 4. watercooled probe, 5. protective gas blowing tube, 6. induction furnace, 7. crucible, 8. rotational disk, 9. motor, and 10. detail of the freeze layer. (The arrow indicates the sampling location for SEM and EPMA.).

Fig. 3—Schematic drawing of the watercooled probe. The arrows indicate the water flow.

furnace, while a protective N_2 atmosphere is blown above the slag (100 l/h). When the targeted bath temperature (1365 °C to 1375 °C) is reached, a sample of the "start slag" bath is taken with a cold steel rod and quenched in liquid nitrogen, in order to prevent oxidation. Next, the thermocouple for measuring the slag bath temperature is removed and the watercooled probe with the two fixed thermocouples is submerged 9 mm into the bath for the prefixed submergence time, to form a freeze layer. During submergence, the rotational speed of the crucible, the water flow rate (4 to 5 l/h), and the furnace power are kept constant. At the end of the experiment, the probe with the freeze layer is removed from the slag bath and cooled in a nitrogen atmosphere. After replacing the slag bath thermocouple and reheating the slag to the starting bath temperature, an "end slag" bath sample is taken, using the same procedure as for the start slag bath sample. When the freeze layer is at room temperature, the thickness of the bottom and the top parts of the freeze layer is measured. Figure 4 shows an example of a freeze layer in which the top and the bottom parts are indicated.
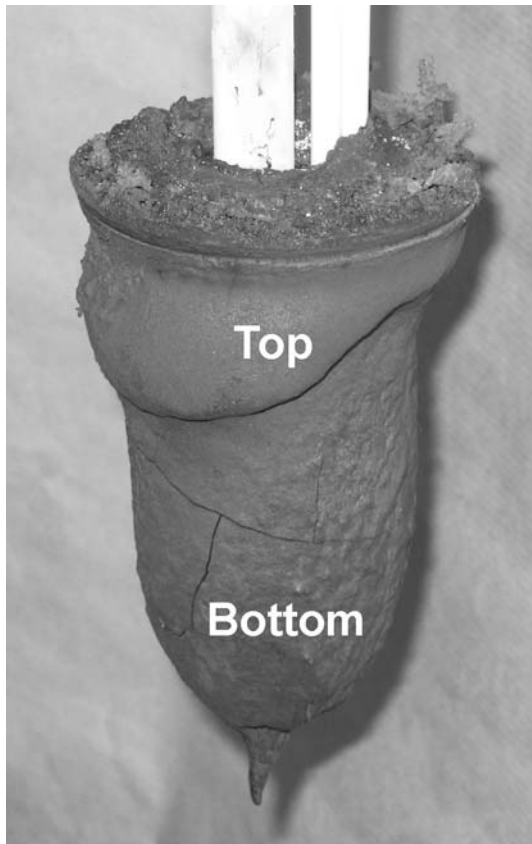
Fig. 4—An example of a freeze layer formed with a watercooled probe technique under base case experimental conditions. The bottom and top parts, in which the thickness of the freeze layer is measured, are indicated.

B. Experiments

Three series of experiments were performed. In each series, either the submergence time, the furnace power, or the rotational speed of the crucible was varied, starting from base case conditions (30-min submergence time, 20-kW furnace power, and 5.7-rpm rotational speed). All the performed experiments are listed in Table I.

C. Analysis

The composition of the slag bath samples is determined by fusing the sample with Na_2O_2 and leaching with HCl. The resulting liquid is analyzed, using inductively coupled plasma–atomic emission spectroscopy (ICP-AES). The Fe^{2+} amount is analyzed by partly dissolving the sample in a HF and H_2SO_4 solution. Some O-phenantroline is added to the solution, to form a complex. The whole is analyzed with ultraviolet-visible (UV-VIS) spectrometry. The Fe^{3+} amount is the difference between total Fe amount and the Fe^{2+} amount. Only the samples of one base case experiment are analyzed for Fe^{2+}.

For scanning electron microscopy (SEM) and electron probe microanalysis (EPMA), a sample is taken at the bottom part of the freeze layer (Figure 2(10)). The SEM is used in backscattered electron (BSE) mode at a 10-kV acceleration voltage. The EPMA, using energy-dispersive spectroscopy (EDS), is performed at a 20-kV acceleration voltage and a beam current of 3 nA. Surface scans of a rectangular area of 500 to 350 μm are performed every 0.5 mm through the freeze layer. The EPMA using wave-length-dispersive spectroscopy (WDS) is performed with a reference current of 30 nA in the willemite standard at a 20-kV acceleration voltage.

The X-ray powder diffraction (XRD) analyses are performed with a monochromator and Cu K_α radiation (45 kV and 40 mA). Only the submergence time samples involving 5 seconds and 60 minutes are examined. The powder samples are taken with a small diamond drill (1.3 mm in diameter), at constant distances (0, 5, 10, 15, and 20 mm) to the probe surface.

D. Industrial Nonferrous Slag

The composition of the industrial nonferrous slag, as-received from the lead blast furnace process, is shown in Table II. Iron is present as Fe^{2+} and Fe^{3+} in the slag. The slag also contains small amounts of minor elements, such as Mn and K, that are not accounted for in Table II.

Table I. Three Series of Performed Experiments with Their Experimental Conditions; the Base Case is Shown Separately

Series of Experiments	Submergence Time	Furnace Power	Rotational Speed	Number of Experiments
Base case	30 min	20 kW	5.7 rpm	3
Influence of submergence time	5 sec	20 kW	5.7 rpm	1
	5 min	20 kW	5.7 rpm	2
	15 min	20 kW	5.7 rpm	2
	45 min	20 kW	5.7 rpm	2
	60 min	20 kW	5.7 rpm	2
Influence of furnace power	30 min	17.5 kW	5.7 rpm	2
	30 min	22.5 kW	5.7 rpm	2
	30 min	25 kW	5.7 rpm	2
Influence of rotational speed	30 min	20 kW	0 rpm	2
	30 min	20 kW	13.8 rpm	2
	30 min	20 kW	28.5 rpm	2

SiO$_2$	CaO	Total Fe	ZnO	MgO	Al$_2$O$_3$
25.60	18.15	26.00	5.41	1.35	6.35

E. *Thermodynamic Calculations*

Thermodynamic calculations are performed with FactSage, using the FACT53 and FACToxid databases.[13] Only the main components, SiO$_2$, CaO, FeO$_x$, ZnO, Al$_2$O$_3$, and MgO, are considered. The slag is assumed not to be in contact with a second phase, such as a gas or a metal, and the amount of oxygen is assumed to remain constant as a function of temperature.

III. RESULTS

First, the results of the slag bath analysis and the calculated equilibrium solidification path are described. Then, the results for the thickness, microstructure, and composition of the freeze layers are shown. For the microstructures and the composition of the freeze layers, the base case and the three series of experiments are considered separately.

A. *Slag*

1. *Start and end slag bath composition*
For the start and end slag bath samples of all experiments, a deviation less than 1 wt pct from the composition in Table II is observed. The Fe^{2+}/Fe^{3+} analysis of the start and end slag bath samples of one base case experiment gives a Fe^{2+}/Fe^{3+} ratio of 10. For the other experiments, a similar ratio is assumed.

2. *Solidification path*
Figure 5 shows the calculated equilibrium solidification path of the slag. As input, the composition in Table II with a Fe^{2+}/Fe^{3+} ratio of 10 is used. The liquidus temperature of the slag is 1232 °C and wüstite forms as primary phase. At 1198 °C, melilite starts to form. The fraction of wüstite and melilite increases simultaneously following the eutectic reaction L $\rightarrow$ W + M. At 1135 °C, spinel starts to form, while the amount of wüstite and melilite increases following the eutectic reaction L $\rightarrow$ W + M + S. At 1111 °C, olivine starts to form, while the fraction of wüstite decreases following the peritectic reaction L + W $\rightarrow$ O. Finally, the last liquid solidifies at 1083 °C. The fractions of solid phases at the solidus temperature are 6.9 wt pct wüstite, 47.5 wt pct melilite, 8.4 wt pct spinel, and 37.2 wt pct olivine.

For slight changes in the slag composition, the fraction of the solid phases slightly changes and, in some cases, the phase formation temperature changes. An addition of MgO results in an increasing olivine formation temperature and an increasing melilite formation temperature. An increase in SiO$_2$ or a decrease in Al$_2$O$_3$ change the spinel formation temperature and result in the formation of spinel as the last phase, instead of olivine.
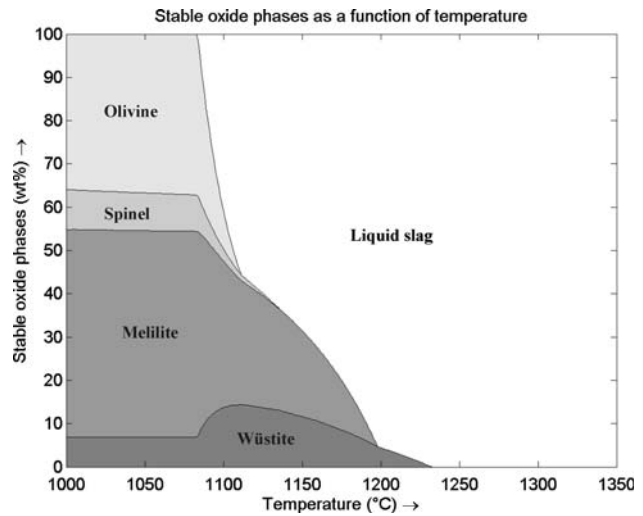

Fig. 5—The equilibrium solidification path of the industrial nonferrous slag for infinitely slow cooling and infinitely fast diffusion in the solid phases. For the calculations, the slag composition in Table II is used, with a Fe^{2+}/Fe^{3+} ratio of 10.

B. *Freeze Layer Thickness*

1. *Submergence time*
The thickness of the freeze layers as a function of submergence time is shown in Table III. In the first 5 minutes, the freeze layer grows rapidly. Between 5 and 15 minutes, the growth slows down; between 15 and 30 minutes, the freeze layer grows only slightly. After 30 minutes, the freeze layer grows faster and the liquid slag bath tends to solidify completely. Both the experimental deviation and the difference between the top and bottom parts increase strongly from 30 minutes, resulting in a conical form and a decrease in the reproducibility.

2. *Furnace power*
With increasing furnace power, the freeze layer thickness decreases, as is shown in Table III. Both the experimental deviation and the difference between the top and bottom parts strongly decrease with furnace power.

3. *Rotational speed*
The freeze layer thickness does not change with rotational speed, as is shown in Table III. There is no influence on the experimental deviation and the difference between the top and bottom parts.

C. *Freeze Layer Microstructure*

1. *Base case*
For the base case experiments, two types of microstructures are observed, which are shown in Figure 6. These two microstructure types are even observed at different locations within a same freeze layer. The phases present are indicated in Figure 7.

In both microstructures, four zones can be distinguished. Zone 1 starts at the probe surface and consists of an amorphous matrix with small wüstite (rounded

Table III. Thickness of the Freeze Layers for the Three Series of Experiments

| Series of Experiments	Varying Parameter	Thickness Bottom $\pm \sigma$	Thickness Top $\pm \sigma$
Influence of submergence time	0 min	0 mm	0 mm
	5 min	14 $\pm$ 1 mm	13 $\pm$ 2 mm
	15 min	19 $\pm$ 4 mm	19 $\pm$ 4 mm
	30 min	21 $\pm$ 5 mm	25 $\pm$ 10 mm
	45 min	33 $\pm$ 13 mm	40 $\pm$ 17 mm
	60 min	32 $\pm$ 15 mm	50 $\pm$ 4 mm
Influence of furnace power	17.5 kW	25 $\pm$ 7 mm	35 $\pm$ 3 mm
	20.0 kW	21 $\pm$ 5 mm	25 $\pm$ 10 mm
	22.5 kW	21 $\pm$ 2 mm	23 $\pm$ 1 mm
	25.0 kW	17 $\pm$ 2 mm	15 $\pm$ 1 mm
Influence of rotational speed	0 rpm	25 $\pm$ 1 mm	26 $\pm$ 6 mm
	5.7 rpm	21 $\pm$ 5 mm	25 $\pm$ 10 mm
	13.8 rpm	23 $\pm$ 1 mm	32 $\pm$ 1 mm
	28.5 rpm	25 $\pm$ 1 mm	29 $\pm$ 2 mm
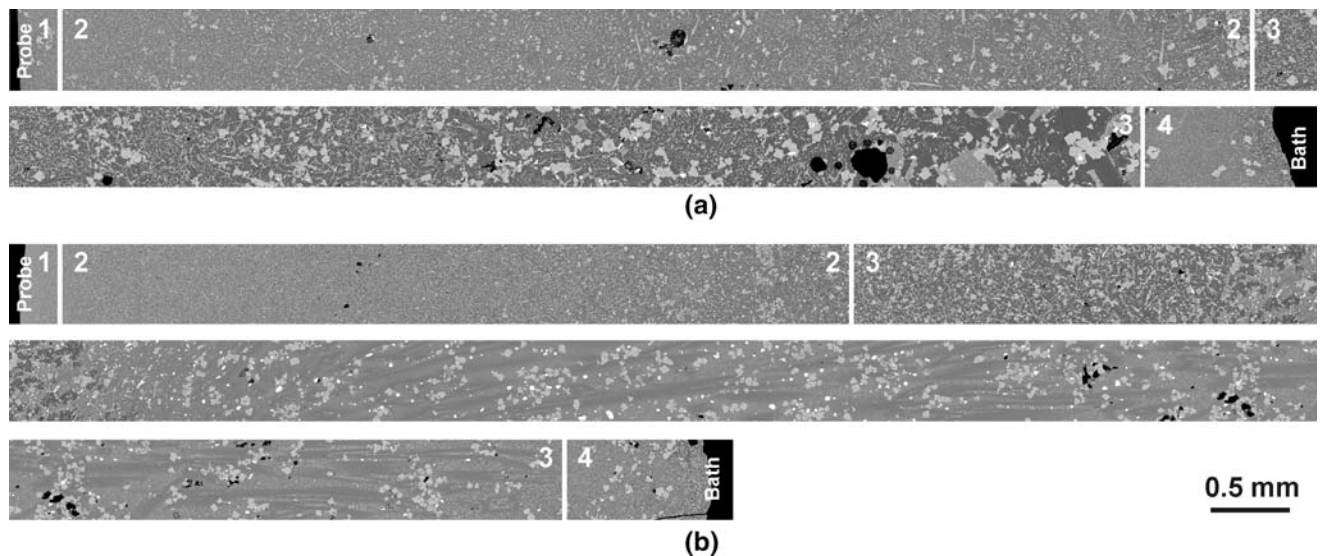
Fig. 6—(a) and (b) The two types of microstructures of the base case experiments. In both, four zones can be distinguished: 1. amorphous matrix with small crystals, 2. equiaxial crystals, 3. columnar crystals, and 4. amorphous matrix with small crystals similar to zone 1. The phases are indicated in Fig. 7.
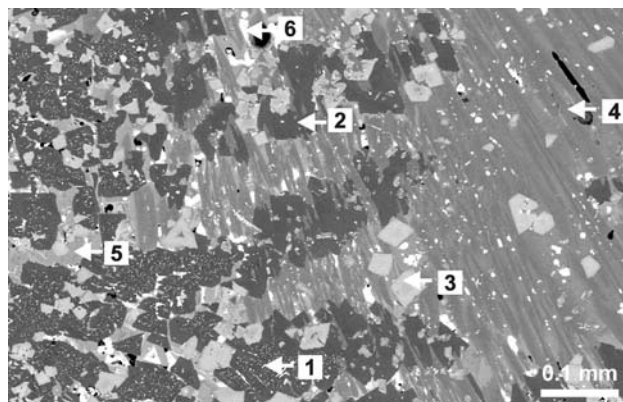

Fig. 7—The phases that can be observed in the microstructures shown in Figs. 6 and 8: 1. dark gray melilite crystals with small light gray wüstite crystals, 2. dark gray melilite crystals, 3. light gray faceted spinel crystals, 4. long thin gray olivine crystals, 5. the amorphous matrix, and 6. white matte droplets.

light gray) and spinel (faceted light gray) crystals. Some spinel crystals are remarkably larger, but their number is limited. In zone 2, equiaxial crystals are observed in an amorphous matrix. These crystals consist of wüstite, melilite (dark gray), spinel, and olivine (long, thin, gray crystals) phases. In zone 3, large crystals, oriented parallel to the heat flux, dominate the microstructure. These are columnar crystals. In one type of microstructure (Figure 6(a)), the columnar crystals consist of melilite phase. Within these melilite crystals, both wüstite and spinel crystals are entrapped. In between, the amorphous matrix with small spinel and wüstite crystals is observed. In the other type of microstructure (Figure 6(b)), the columnar crystals initially consist of melilite phase, but further from the probe, the olivine phase appears. Within the olivine columnar crystals, only spinel crystals are entrapped. In between, the amorphous matrix with small spinel and wüstite crystals

is observed. Zone 4 is located at the liquid bath side and consists of an amorphous matrix with small wüstite and spinel crystals and, in some microstructures, also with small melilite crystals.

During the experiment, the phase indicated as the amorphous matrix in the four zones was a liquid or a glass. Unfortunately, the liquid transforms to a glass after the sample is cooled down and the original interface between liquid and glass cannot be determined *ex situ*.

2. Submergence time

The microstructure as a function of submergence times (5 seconds, and 5, 15, 30, 45, and 60 minutes) is shown in Figure 8. The figure shows only parts of the microstructure at different distances to the probe.

In all microstructures, except for the 5-second sample, the four zones can also be distinguished. Zone 1 already forms before the 5 seconds of submergence time. In some microstructures, the small wüstite and spinel crystals are slightly larger than in others, but no effect of time is observed. In some microstructures, larger spinel crystals are observed, but their presence is also independent of time. Zone 2 forms already before the 5 minutes of submergence time. No effect of submergence time is observed. Zone 3 also forms before the 5 minutes of submergence time. The columnar crystals coarsen and the length of the zone increases with the submergence time. Both melilite and olivine columnar crystals appear for all submergence times. In zone 4, no influence of submergence time is observed.

3. Furnace power

In relation to furnace power, the four zones can again be distinguished. In zones 1 and 2, the microstructure does not change with increasing furnace power. In zone 3, with increasing furnace power, the columnar crystals coarsen and the length of the zone becomes shorter. Both melilite and olivine columnar crystals are observed for all furnace power values. The microstructures of the 17.5-kW samples have a fifth zone. In this zone, large equiaxial melilite crystals are present. Some spinel and wüstite crystals are entrapped in the melilite crystals. In between, the amorphous matrix with small crystals is present. The melilite crystals in zone 4 are much larger for 17.5-kW furnace power.

4. Rotational speed

Similar to the microstructures of the base case freeze layers, four zones can be distinguished for rotational speed. In zones 1 and 2, there is no effect of rotational speed on the microstructure. The thickness of zone 2, however, decreases with increasing rotational speed. In zone 3, it is noticeable that, for higher rotational speeds, only the microstructure type with olivine crystals is observed. The thickness of zone 3 increases for higher rotational speeds. On zone 4, there is no effect.

D. Composition Profiles through the Freeze Layers

1. Base case

Figure 9 shows the composition profiles through the freeze layers of both microstructure types. In zones 1 and 2, the composition of the freeze layer is constant. Zone 3 of the microstructure type with melilite columnar crystals (Figure 9(a)) seems to show a small concentration gradient: a decrease of 5 wt pct FeO and small increases of 3 wt pct SiO_2 and 3 wt pct CaO. Zone 4 of this microstructure shows an opposite concentration gradient: an increase of 5 wt pct FeO and decreases of 3 wt pct SiO_2 and 3 wt pct CaO. The microstructure type with olivine columnar crystals does not show a gradient, and the composition in zones 3 and 4 equals the composition in zones 1 and 2 (Figure 9(b)).

2. Submergence time

In zones 1 and 2, the composition of the freeze layer remains constant with the submergence time. In zone 3, however, for short submergence times (5 to 15 minutes), no gradient is seen; for longer submergence times, a gradient similar to the one in Figure 9(a) appears. The FeO-concentration decreases, while the SiO_2 and CaO concentration increases. Here the microstructures consist of melilite or a combination of melilite and olivine. In zone 4, an opposite gradient is seen for the longer submergence times.

3. Furnace power

There is no influence of furnace power on the composition of the freeze layer in zones 1 and 2. For 25 kW, a gradient is observed in zone 3, which consists of melilite columnar crystals. The gradients are similar to the ones for 20 kW in Figure 9(a).

4. Rotational speed

The rotational speed has no effect on the composition of the freeze layer. All profiles are similar to the one in Figure 9(b) for 0, 13.8, and 28.5 rpm.

IV. DISCUSSION

In the following subsections, first, the freeze layer formation will be discussed extensively. Next, the influence of the heat input in the slag bath and the convection on the freeze layer are discussed. Then, the stability of the watercooled probe technique is evaluated. Finally, the implications for freeze lining applications are considered.

A. Freeze Layer Formation

The microstructure of a freeze layer strongly depends on the distance to the probe. Different zones form in which different mechanisms dominate the growth morphology and the scale of the microstructure. According to general solidification theory, the growth morphology and the scale of the microstructures strongly depend on the solidification rate (V) and the temperature gradient at the solid-liquid interface (G).[14] The ratio G/V determines the growth morphology: from a high to a low ratio, first a planar front forms, then columnar crystals without any branches appear, followed by columnar crystals with branches, called dendrites, and, finally, equiaxial crystals form.
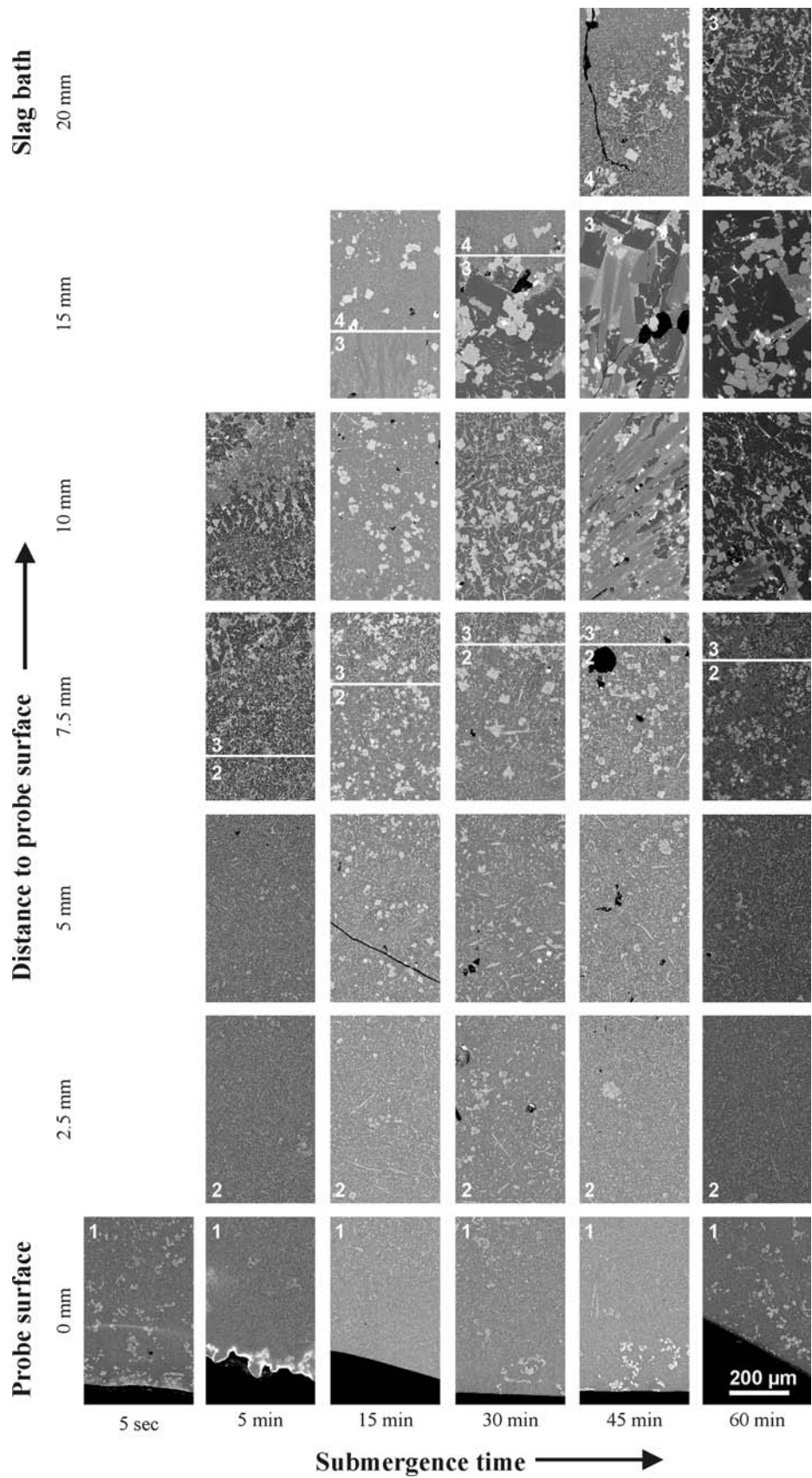
Fig. 8—The microstructure as a function of submergence time (5 s, and 5, 15, 30, 45, and 60 min). Only fragments of the microstructure at the indicated distance to the probe are shown. The different zones are indicated on the figure.
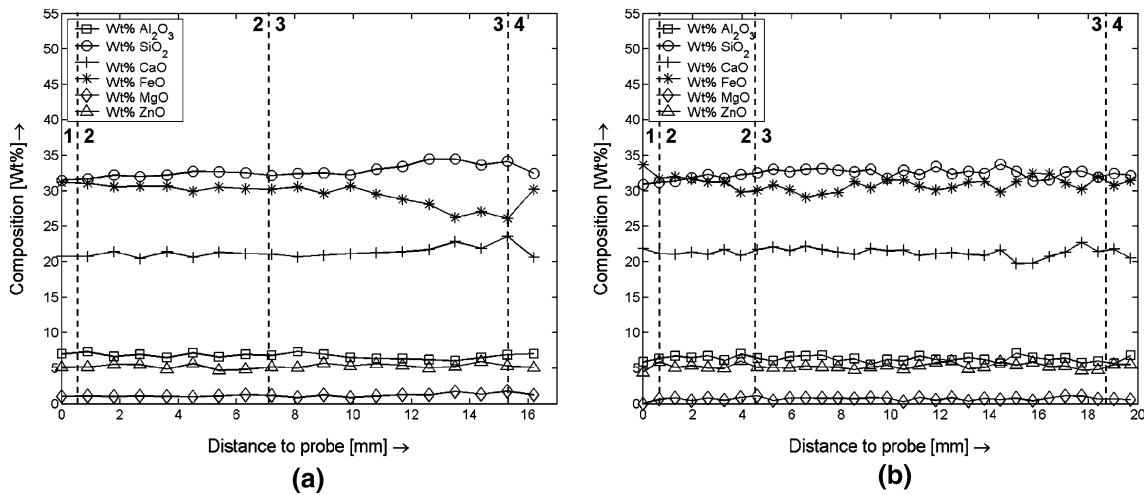
Fig. 9—Composition profiles through the freeze layers of the base case experiments. (*a*) the microstructure type with melilite columnar crystals (Fig. 6(*a*)) and (*b*) the microstructure type with olivine columnar crystals (Fig. 6(*a*)). The four zones are indicated in the graphs.

The product $G·V$ determines the scale of the microstructure: high values give fine grains, while low values give coarse grains.

During a watercooled probe experiment, both are continuously changing. The first slag that solidifies is in immediate contact with the cooled probe and is quenched very fast to a low temperature. This slag layer insulates the cooled probe, so the next slag layer solidifies more slowly and will finally be at a higher temperature. The temperature evolutions at different distances to the probe are schematically shown in Figure 10 (black curves in graph).

Furthermore, the solidified slag is annealed at an increasing annealing temperature for an increasing distance to the probe, as is shown for the larger submergence times, in Figure 10. Thus, depending on the location in the freeze layer, the microstructure can further coarsen with time.

In the following subsections, the formation of the four zones in the microstructure will be discussed in more detail.

In zone 1, the liquid slag is rapidly quenched on the cooled probe surface and the cooled probe is in almost direct contact with the hot slag bath, resulting in a low G/V ratio and a high $G·V$ value. As a result, the microstructure consists of an amorphous phase with a small fraction of wüstite and spinel crystals. The composition of the freeze layer in this zone equals the bath composition.

The small crystals form during the quenching of the slag. In some microstructures, these crystals are slightly larger. The change in size is, however, not related to submergence time; thus, it is not due to annealing of the crystals. More likely, the freeze layer does not always make a good contact with the probe and the slag is, in some cases, less rapidly quenched, so slightly coarser crystals can form. Some microstructures also contain larger spinel crystals, which were probably already present in the liquid slag bath.

In zone 2, the G/V is higher and the $G·V$ is lower than in zone 1, so equiaxial crystals, which are larger than in
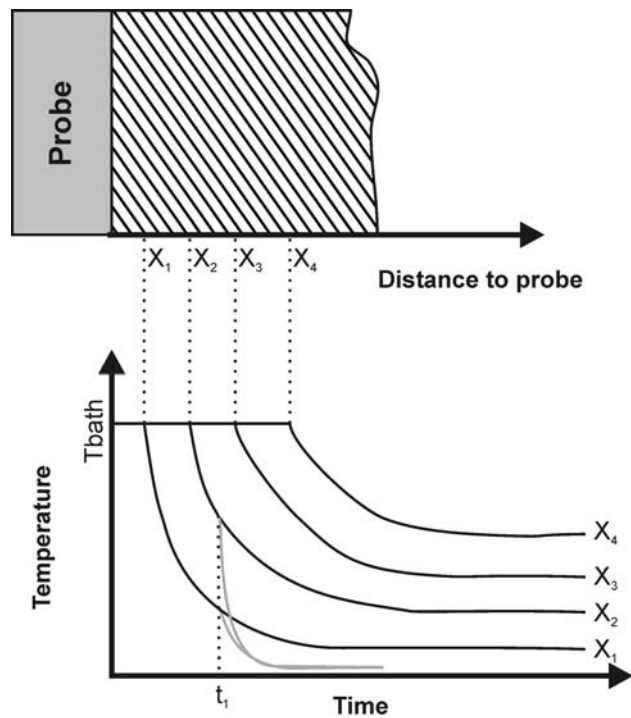

Fig. 10—Schematic drawing of the temperature evolution in the freeze layer as a function of time for different distances (x_1 through x_4) to the probe surface. The black curves are the evolutions during the experiment, and the gray curves are the evolutions after removing the probe from the liquid bath at time t_1 and during cooling down to room temperature.

zone 1, can form. These crystals consist of wüstite, melilite, spinel, and olivine phase. In between, amorphous matrix is present, which was immediately glassy during formation of the zone. Although this zone is at a higher temperature than zone 1, no annealing effect is observed here, as well. The composition of this zone equals the composition of the slag bath.

In zone 3, the G/V increases further, so columnar crystals can form. The formation of columnar crystals

implies that, apart from heat transport, mass transport controls the growth of the layer. If the solidification rate is much higher than the mass transport rate, the heat transfer determines the growth of the layer. However, for solidification rates with a similar or a lower magnitude than the mass transport rate, concentration gradients appear in the liquid at the solid-liquid interface. If these gradients result in a local liquidus temperature at the solid-liquid interface that is higher than the local temperature, an area of constitutional undercooling forms, resulting in columnar growth.[14] Since the $G \cdot V$ decreases with increasing thickness of the freeze layer, larger columnar crystals form.

Two microstructure types form. For both, initially columnar crystals of the melilite phase form but, in one type at a certain moment, olivine columnar crystals form and from then on dominate the microstructure. From the results, it is not clear why both types form.

The columnar crystals do not form first. The entrapment of large spinel crystals, which are not homogeneously distributed in the olivine crystals, indicates that they were present before the columnar crystals. Only in the melilite crystals are also wüstite crystals entrapped. This microstructure is typical for the eutectic reaction L → W + M (Figure 5). In the olivine columnar crystals, no entrapped wüstite crystals are observed. According to the solidification path, the fraction wüstite decreases when olivine starts to form, due to a peritectic reaction.

For larger submergence times, the composition of the freeze layer in zone 3 differs slightly from the composition of the bath, according to the composition profiles. A small decrease in FeO concentration and a small increase in SiO_2 and CaO are observed. These gradients are caused by an exchange of components between the freeze layer and the liquid slag bath. An exchange of components with the bath is likely, because the columnar crystals have a different composition from the slag bath. In between the columnar crystals, however, bath material is entrapped, so the freeze layer composition differs only slightly from the bath composition.

In zone 4, an amorphous matrix with small crystals is observed. Since columnar crystals only form in a liquid phase,[14] it is concluded that this zone consists of liquid slag that sticks to the freeze layer when removing the probe from the liquid slag bath and that is quenched in air.

After removing the probe from the liquid slag bath, the freeze layer cools fast down to room temperature. The temperature evolution is shown by the gray lines in Figure 10, starting from time t_1. This cooling is assumed to have only a limited effect on the microstructure.

B. Influence of Heat Input from Bath

With increasing furnace power, a higher slag bath temperature can be maintained. A higher bath temperature results in an increase in heat input from the bath to the freeze layer. As a result, the freeze layer becomes thinner and the solidification rate is lower. A higher bath temperature also results in a higher temperature gradient at the freeze layer-liquid bath interface. Both the growth morphology and the scale of the microstructure are thus affected.

The same four zones as are in the base case can also be distinguished in all the microstructures. Zones 1 and 2 are similar, but in zone 3, the columnar crystals coarsen. The coarsening of the columnar crystals with furnace power is due to a decrease in $G \cdot V$. Zone 3 is less thick, with increasing furnace power. Zone 4 only differs for the 17.5 kW and contains large melilite crystals. In this microstructure, a fifth zone is also observed, with large equiaxial melilite crystals. Probably here the liquid slag bath was undercooled (bath temperature lower than liquidus temperature) and the melilite crystals already form in the liquid bath.

The two microstructure types appear for both low furnace power and high furnace power. Thus, a difference in thermal conditions can only be a part of the explanation.

C. Influence of Convection in Bath

The rotational speed of the crucible affects the convection in the liquid slag bath. For 0 rpm, only free convection appears. This free convection might be high, since there are strong temperature gradients present in the liquid slag. With increasing rotational speed, a forced convection term is added. To determine the impact of the added forced convection, the ratio of the Grashof number (Gr) to the square of the Reynolds number (Re) is used:[15]

$$\frac{\text{Gr}}{\text{Re}^2} = \frac{g * \beta * (T_s - T_\infty) * L}{u^2}$$

with g the gravitational acceleration, β the volumetric thermal expansion coefficient, T_s the temperature at the freeze layer surface, T_∞ the slag bath temperature, L the distance between the freeze layer and the crucible, and u the average flow rate in the bath. For a ratio much higher than one, free convection dominates; for a ratio much smaller than one, forced convection dominates. For the present experiments, assuming $T_s - T_\infty$ to be 200 K (approximately the difference between the bath temperature and the melilite formation temperature) and β to be 10^{-4} 1/K,[16] 28.5 and 5.7 rpm give a ratio of circa 0.5 and of circa 25, respectively. Thus, forced convection has an impact similar to that of free convection, for the higher rotational speeds.

An increase in convection in the slag bath results in an increase in the heat convection coefficients between the bath and freeze layer and between the bath and crucible, in steeper temperature and concentration gradients at the solid-liquid interface, and in an increase in the convective mass transport in the slag bath. The effect on the solidification rate is not clear.

The results show that the thickness of the freeze layer is more or less constant with increasing rotational speed; thus, in the experiments, the impact on the solidification rate is limited. The thickness of zones, however, changes. Zone 2 seems to shorten, while zone 3 seems to thicken, which is probably a combined effect of increasing G/V and a higher mass transport relative to the solidification rate.

The rotational speed seems to have an influence on the microstructure type that forms. For high rotational speeds, only microstructures with olivine columnar crystals are observed. Thus, the mass transport seems to be of major importance for the selection of microstructure type.

D. *Experimental Technique*

The formation of two microstructure types for similar experimental conditions might imply that the experimental setup operates in an unstable mode. However, the submergence time and furnace power do not favor one microstructure type, the thickness of the freeze layer is well reproducible for most experiments, and the two microstructure types are observed within the same freeze layer. Thus, in one experiment, the conditions (such as temperature and composition) can change for different locations at the freeze layer surface, resulting in the formation of the different microstructure types.

For the performed experiments, the equilibrium thickness of the freeze layer is not reached. The cooling by the probe was too strong compared to the heat input from the liquid slag bath. This caused complete solidification of the slag bath for long submergence times and low furnace powers, and the thickness of the freeze layer was difficult to reproduce. In the future, working with a less intensive cooling probe, such as a gas-cooled probe, is recommended.

E. *Implications for Freeze Lining Applications*

The results imply that the microstructure of a freeze layer is strongly influenced by the temperature and the composition of the liquid slag at the freeze layer surface. Changing thermal conditions influence the solidification rate of the freeze layer and the temperature gradient at the freeze layer-bath interface, leading to the formation of zones with different growth morphology and scale. Depending on the solidification rate, the composition at the freeze layer-bath interface can change, resulting in a concentration gradient in the bath at the freeze layer surface, which affects the growth morphology. Furthermore, when thermal conditions and the bath composition vary locally at the freeze layer surface, different microstructures types may form. To understand the formation and the evolution of the microstructure, it is important to understand the effect of local thermal history, of local mass transport, and of local composition.

The local microstructure affects the local properties of the freeze layer and, therefore, its stability and performance. For example, the melting of the freeze layer will be influenced: a glass phase with the same composition as the slag bath will melt more easily than large crystals of a phase with a different composition from the bath.

The microstructures of the freeze layers of the studied industrial nonferrous slag are not dominated by crystals of primary phase. For none of the freeze layer studied is an increase in primary phase observed. Instead, the secondary or last phase to form keeps dominating

the microstructure. Furthermore, it was expected that the freeze layer enriches in FeO, since wüstite consist mainly of FeO. The composition profiles, however, show the opposite behavior. This implies that the freeze layer surface temperature does not equal the liquidus temperature of the slag bath during freeze lining formation.

V. CONCLUSIONS

In order to study the microstructure and the composition of an industrial nonferrous slag freeze lining, three series of experiments are performed. Starting from base case conditions, the submergence time of the probe, the furnace power, and the rotational speed of the crucible are varied to study the formation of the freeze layer, the effect of heat input from the slag bath, and the effect of convection in the slag bath.

During freeze lining formation, the solidification rate and the temperature gradient at the freeze layer-bath interface are continuously changing, resulting in the formation of different zones. First, a zone consisting of an amorphous matrix with small precipitates forms, followed by a zone with equiaxial crystals. Finally, a zone with columnar crystals forms. The microstructure coarsens with distance to the probe. An increase in heat input from the slag bath results in the formation of thinner freeze layers. The same growth morphologies can still be identified in all microstructures. An increase in rotational speed favors the growth of columnar crystals, and they start to form at shorter distances to the probe.

Furthermore, two microstructure types are observed, which show different phases for the columnar crystals. In one microstructure type, melilite columnar crystals form, while in the other microstructure type, olivine columnar crystals form. These types form under similar experimental conditions and are even observed within the same freeze layer. Submergence time and furnace power do not seem to favor either microstructure type. The rotational speed of the crucible and, thus, the convection in the liquid slag do seem to have an influence.

REFERENCES

1. L.R. Nelson, R. Sullivan, P. Jacobs, E. Munnik, P. Lewarne, E. Roos, M.J.N. Uys, B. Salt, M. de Vries, K. McKenna, N. Voermann, and B.O. Wasmund: *J. S. Afr. Inst. Min. Metall.*, 2004, vol. 104 (9), pp. 551–61.
2. D.G.C. Robertson and S. Kang: *Fluid Flow Phenomena in Metals Processing*, San Diego, CA, 1999, TMS, Warrendale, PA, 1999, pp. 157–68.
3. K. Verscheure, M. Van Camp, B. Blanpain, P. Wollants, P. Hayes, and E. Jak: *Metall. Mater. Trans. B*, 2007, vol. 38B, pp. 13–20.
4. K. Verscheure, M. Van Camp, B. Blanpain, P. Wollants, P. Hayes, and E. Jak: *Metall. Mater. Trans. B*, 2007, vol. 38B, pp. 21–33.
5. J.H. Zietsman and P.C. Pistorius: *Miner. Eng.*, 2006, vol. 19, pp. 262–79.
6. P.C. Pistorius: *Proc. VII Int. Conf. on Molten Slags, Fluxes and Salts*, Cape Town, South Africa, 2004, SAIMM, Johannesburg, South Africa, 2004, pp. 237–42.

7. P.C. Pistorius: *J. S. Afr. Inst. Min. Metall.*, 2003, vol. 103 (8), pp. 509–14.
8. K.A. Rye, T. Eidet, and K. Tørklep: *Light Metals 1999*, San Diego, CA, 1999, TMS, Warrendale, PA, 1999, pp. 347–52.
9. C.C. Wei, J.J.J. Chen, B.J. Welch, and V.R. Voller: *Light Metals 1997*, Orlando, FL, 1997, TMS, Warrendale, PA, 1997, pp. 309–16.
10. A. Solheim and L.I.R. Støen: *Light Metals 1997*, Orlando, FL, TMS, Warrendale, PA, 1997, pp. 325–32.
11. J. Thonstad and S. Rolseth: *Light Metals 1983*, New York, NY, 1983, TMS-AIME, Warrendale, PA, 1983, pp. 415–23.
12. K. Verscheure, M. Campforts, F. Verhaeghe, E. Boydens, M. Van Camp, B. Blanpain, and P. Wollants: *Metall. Mater. Trans. B*, 2006, vol. 37B, pp. 929–40.
13. C.W. Bale, P. Chartrand, S.A. Degterov, G. Eriksson, K. Hack, R. Ben Mahfoud, J. Melançon, A.D. Pelton, and S. Petersen: *Calphad*, 2002, vol. 26 (2), pp. 189–228, www.factsage.com.
14. W. Kurz and D.J. Fisher: *Fundamentals of Solidification*, 3rd ed., Trans Tech Publ, Aedermannsdorf, 1989.
15. F.P. Incropera and D.P. DeWitt: *Fundamentals of Heat and Mass Transfer*, 5th ed., John Wiley & Sons, New York, NY, 2002, p. 539.
16. K.C Mills: *ISIJ Int.*, 1993, vol. 33 (1), pp. 148–55.